CHEMICAL PHYSICS

Waveform-dependent air fluorescence from neutral and ionic nitrogen molecules

Hao Liang[1]*†, Ming-Shian Tsai[2]†, Chun-Chia Tseng[2], Ming-Chang Chen[2]*, Uwe Thumm[3], Meng Han[3]*

Laser-induced air fluorescence in the ultraviolet regime is primarily attributed to transitions between the C and B states in excited neutral N_2 molecules and between the B and X states in N_2^+ ions. However, the mechanism underlying the former remains contentious, as direct population to the C state by light fields is forbidden by electron spin constraints. In this work, we investigate the mechanism of air fluorescence from excited neutral N_2 molecules by carrier-envelope phase–stabilized sub–4 femtosecond pulses. Our results show that fluorescence from N_2^+ ions reaches a maximum with cosine-like pulses, while fluorescence from excited neutral N_2 molecules peaks with sine-like pulses. In addition, by scanning the chirp of the driving pulse, we find that ionic fluorescence is maximized with chirp-free pulses, whereas neutral fluorescence favors negatively chirped pulses. These observations, supported by classical trajectory Monte Carlo simulations, support the mechanism of intersystem crossing from excited spin-singlet states, which are populated via recollision-induced strong-field excitation.

INTRODUCTION

Lightning is a natural phenomenon characterized by electrostatic discharges between electrically charged regions in the atmosphere, producing a bright flash. Similarly, ultrashort and intense light pulses can, under certain conditions, replicate this effect. When intense femtosecond laser pulses are focused in ambient air, the strong electric field can ionize atomic and molecular species—mainly nitrogen molecules (N_2)—through multiphoton and tunneling ionization, creating a bright plasma filament composed of hot electrons, ions, and excited neutral species. This laser-induced filamentation results from nonlinear light-molecule interaction and emits secondary radiation across a wide frequency range, including high-order harmonics (*1*), terahertz radiation (*2*–*4*), and radio frequency waves (*5*, *6*). Among these, fluorescence, originating from the noncoherent radiative relaxation of the population in the excited states, stands out as an important emission because of its background-free and easily accessible nature. Air fluorescence has enabled innovative spectroscopic applications, such as remote sensing of pollutants and hazardous materials (*7*, *8*). During filamentation, nitrogen molecules—both neutral and ionic—emit readily observable fluorescence. The formation of N_2^+ is likely due to multiphoton and tunneling ionization during the laser pulse. However, the mechanism responsible for the formation of the spin-triplet state in excited neutral N_2 is less clear and remains under debate, as direct excitation into this state by light fields is spin-forbidden and thus improbable.

Over the past two decades, researchers have introduced three primary mechanisms to explain the formation dynamics of the excited $C^3\Pi_u$ state (spin triplet) from the ground state (spin singlet) of N_2 molecules. (i) The first mechanism involves collisions of N_2^+ ions with neutral N_2 molecules, forming an N_4^+ intermediate that subsequently dissociates into the $C^3\Pi_u$ state and a ground-state N_2 upon electron attachment (*9*, *10*). This process can be represented as $N_2^+ + N_2 \Rightarrow N_4^+$ and $N_4^+ + e^- \Rightarrow N_2(C^3\Pi_u) + N_2$. We refer to this as the "cation pathway." (ii) The second mechanism is based on electron impact excitation caused by inelastic collisions with hot electrons (*11*–*14*), expressed as $N_2 + e^-(\text{high kinetic energy}, E_k) \Rightarrow N_2(C^3\Pi_u) + e^-(\text{low } E_k)$, which we refer to as the "electron pathway." It has been observed that in very intense circularly polarized infrared fields, fluorescence from the $C^3\Pi_u$ state is stronger than that in linearly polarized infrared fields, likely due to the increased kinetic energy of hot electrons in circular polarization (*12*). (iii) The final mechanism involves the intersystem crossing scenario (*15*). In this case, spin-singlet states of N_2 are first excited by the laser field and then undergo a collision-induced transfer to the spin-triplet, as represented by $N_2^*(\text{spin-singlet}) + M \Rightarrow N_2(C^3\Pi_u) + M$, where M is mainly the N_2 molecule. We refer to this as the "excited neutral pathway."

In principle, determining the dominant mechanism in air fluorescence should be straightforward if one can establish that the fluorescence intensity from the $C^3\Pi_u$ state is proportional to the densities of N_2^+, electrons, or N_2^*. Each mechanism relies on inelastic scattering between different particles and N_2 molecules to excite them from the ground state to the C state, so that identifying such proportionality could clarify which mechanism prevails. Experimentally, however, this approach is challenging. The densities of all three species—N_2^+, electrons, or N_2^*—tend to increase or decrease together with most experimental parameters, such as light intensity of the driving field. Thus, it is crucial to identify an experimental "knob" that selectively increases the density of one species while decreasing or leaving unchanged the densities of the others. Note that the collisional formation of the C state typically occurs on a much longer timescale than the optical pulse duration. However, the short optical pulse influences the density of particles responsible for collisional excitation in the plasma filament, ultimately affecting the population of the C state.

In this work, we observe that the subcycle electric-field waveform strongly influences air fluorescence from both neutral N_2 molecules and N_2^+ ions. By generating and measuring air fluorescence using carrier-envelope phase (CEP)–stabilized sub–4 fs pulses featuring controllable chirps, we provide a means to evaluate each pathway's

[1]Max Planck Institute for Physics of Complex Systems, Nöthnitzer Straße 38, Dresden 01187, Germany. [2]Institute of Photonics Technologies, National Tsing Hua University, Hsinchu 300044, Taiwan. [3]J. R. Macdonald Laboratory, Kansas State University, Manhattan, KS 66506, USA.
*Corresponding author. Email: liangh@pks.mpg.de (H.L.); mingchang@mx.nthu.edu.tw (M.-C.C.); meng9@ksu.edu (M.H.)
†These authors contributed equally to this work.

contribution. We observe that the fluorescence from neutral N_2 molecules shows distinct CEP and chirp dependencies compared to the fluorescence from N_2^+ ions. Using classical trajectory Monte Carlo (CTMC) simulations (*16*), we find that these fluorescence characteristics from neutral N_2 molecules align closely with the population of excited singlet states produced via recollision-induced strong-field excitation. Thus, among the proposed mechanisms, the excited neutral pathway provides the most consistent explanation for the observed waveform-dependent fluorescence driven by few-cycle pulses.

RESULTS

The laser system used in this experiment is a CEP-stabilized Yb laser (PHAROS). We postcompressed the pulse duration to 3.7 fs (full width at half maximum of the intensity envelope) using cascaded four-pass cells (*17*), as characterized by a transient-grating frequency-resolved optical gating. CEP stabilization is actively maintained with both fast and slow feedback loops, achieving a stability of more than 100 mrad in standard deviation over 14 hours, which is critical for observing CEP-dependent contrast at around 1%. See the Supplementary Materials for pulse characterization and CEP performance. The CEP value is determined using an f-to-2f interferometer, with absolute calibration achieved by referencing to the laser-acoustic wave intensity (*18*), where the acoustic intensity maximum is achieved at the cosine-like pulses, corresponding to a CEP of 0 or π. Therefore, our absolute CEP calibration has the ambiguity of π. For pulse chirp variation, we adjusted the thickness of a fused-silica wedge pair (2.8 degrees) inserted into the beam path. Our initial light pulse is negatively chirped by custom-designed chirped mirrors before entering the wedge pair, where the fused silica introduces positive dispersion to modify the chirp. A piezoelectric stage precisely controls the wedge insertion. In the air fluorescence experiments, we used ~100 μJ of the linearly polarized light pulse, split off by a reflection from a fused-silica wedge prism. The pulse was focused by a silver concave mirror with the focal length of 10 cm, achieving an estimated peak intensity of 10^{14} W/cm^2. We used a silicon-based spectrometer with a 150-μm–diameter fiber to collect side-emission fluorescence as a function of laser CEP and wedge insertion. The Gouy phase effect was minimized by using the small-diameter collection fiber.

Figure 1A shows a typical air fluorescence spectrum measured in the ultraviolet regime, which can be categorized into two main types. The most dominant peaks are the transitions from the $C^3\Pi_u$ state to the $B^3\Pi_g$ state in neutral N_2 molecules, such as 337 nm ($\nu = 0 \rightarrow \nu' = 0$), 358 nm ($\nu = 0 \rightarrow \nu' = 1$), and 316 nm ($\nu = 1 \rightarrow \nu' = 0$). ν and ν' designate the vibrational quantum numbers of the upper and lower states, respectively. The second category is the transition from the B state to the X state in N_2^+ ions, such as 391 nm ($\nu = 0 \rightarrow \nu' = 0$), 428 nm ($\nu = 0 \rightarrow \nu' = 1$), and 357 nm ($\nu = 1 \rightarrow \nu' = 0$), with the latter overlapping the neutral signal. Figure 1B presents a schematic illustration of the relevant energy levels. The ionic B state is likely populated by strong-field tunneling ionization, whereas the formation mechanism of the neutral C state remains uncertain. Figure 1C displays the measured CEP-resolved differential distribution of the fluorescence spectrum defined by $[Y(\mathrm{CEP},\lambda) - \overline{Y}(\lambda)]/\mathrm{Max}[]\overline{Y}(\lambda)$, where $Y(\mathrm{CEP},\lambda)$ is the CEP- and wavelength (λ)–resolved fluorescence intensity and $\overline{Y}(\lambda)$ is the CEP-averaged fluorescence intensity. The ionic fluorescence lines at 391 and 428 nm reach their maxima at a CEP of 0,

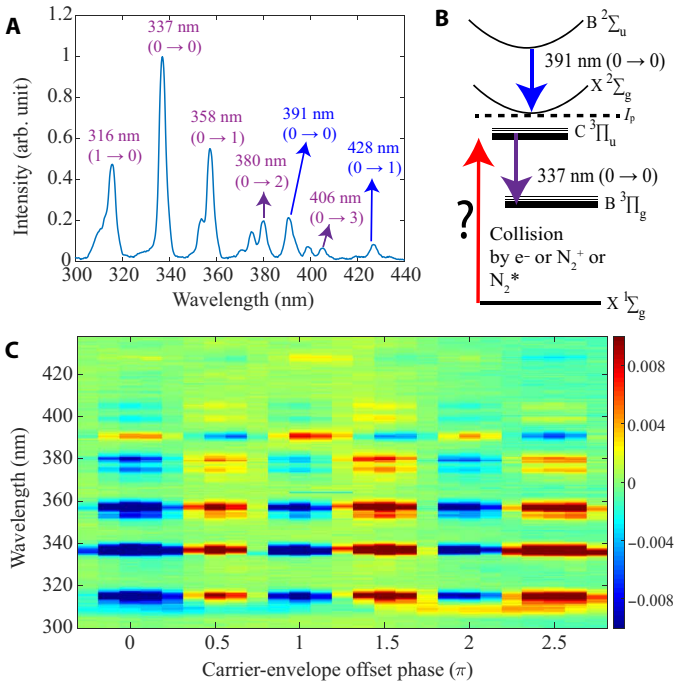

Fig. 1. Assignment of air fluorescence and its CEP dependence. (**A**) Measured typical side-emission air fluorescence spectrum. The peaks not labeled in the plot include 375 nm ($\nu = 1 \rightarrow \nu' = 3$), 371 nm ($\nu = 2 \rightarrow \nu' = 4$), and 399.5 nm ($\nu = 1 \rightarrow \nu' = 4$) from N_2^*. (**B**) Energy diagram of relevant states of excited neutral and ionic N_2 molecules. (**C**) Measured CEP-resolved differential distribution of the fluorescence spectrum defined by $[Y(\mathrm{CEP},\lambda) - \overline{Y}(\lambda)]/\mathrm{Max}[\overline{Y}(\lambda)]$. Note that the limits of the color bar are set to visualize the weak oscillations at 391 and 428 nm, and thus, the signals from N_2^* are saturated. See the Supplementary Materials for the raw data with an unsaturated color bar.

corresponding to a cosine-like pulse. This behavior is expected, as cosine-like pulses produce the highest electric field strength, maximizing the ion yield for the B state. Our results show that all neutral signals are synchronized and reach their maxima at a CEP of π/2, corresponding to a sine-like pulse. Although sine-like pulses minimize the total ionization yield, they enhance the likelihood of recollision events. In addition, the CEP contrast for the neutral signal is markedly higher than that for the ionic signal, prompting us to adjust the color scale limits of Fig. 1C to better visualize the ionic signal. See the Supplementary Materials for $Y(\mathrm{CEP},\lambda)$ with an unsaturated color bar. A pronounced CEP dependence generally indicates a process sensitive to carrier waves under the intensity envelope, such as high-harmonic generation (*19*). We also emphasize that CEP-dependent fluorescence only becomes observable with few-cycle pulses (i.e., <2 optical cycles). In this regime, cosine pulses yield higher ionization but fewer electron returns, while sine pulses produce lower ionization yet more efficient electron recollision with the parent ion. For longer pulses, CEP effects are washed out because of averaging over multiple optical cycles. The modest ~1% CEP contrast observed in our study is therefore limited by the current pulse duration, and we expect stronger CEP sensitivity with even shorter pulses.

In addition to their distinct CEP dependence, we observed that the neutral and ionic fluorescence signals exhibit different responses to pulse chirp. The initial light pulse was negatively chirped, and we

adjusted the chirp by varying the thickness of fused silica inserted into the beam path. Figure 2A shows the measured chirp-resolved differential distribution of the air fluorescence spectrum, defined as $[Y(\text{insertion}, \lambda) - \overline{Y}(\lambda)]/\text{Max}[]\overline{Y}(\lambda)$. The wedge insertion was calculated as the stage position multiplied by tan(2.8°). Note that we varied the wedge insertion in a large step size (34 μm) and the statistic is not enough to resolve the CEP dependence (around 1%) here. Figure 2B shows the lineouts at different wavelengths for comparison. The ionic signals at 391 and 428 nm reach their maximum intensity at a fused silica thickness of 0.9 mm, corresponding to chirp-free pulses. The chirp-free pulse gives the shortest duration and the highest peak intensity. In contrast, the neutral signals at 337 and 316 nm are enhanced when using negatively chirped pulses. Furthermore, the ionic signals display near symmetry with respect to the sign of the pulse chirp and decay more rapidly than the neutral signals. In contrast, the neutral signals exhibit a more asymmetric response to the pulse chirp.

DISCUSSION

The fluorescence from N_2^+ is closely tied to the ionization probability leading to the B state of N_2^+. In contrast, the fluorescence from N_2^* depends on the yields of various particles for different pathways. The electron pathway requires ionized electrons with kinetic energy higher than the 12.0-eV threshold (*20*) of impact excitation of the $C^3\Pi_u$ state. The excited neutral pathway depends on the population of N_2^* in high Rydberg states with energies above the $C^3\Pi_u$ state, while the cation pathway is proportional to the total density of N_2^+. Each of these pathways is influenced by the energy distribution resulting from the photoionization and excitation processes in N_2, which we evaluate numerically using a CTMC simulation (see the Supplementary Materials for details).

The simulated electron energy distribution is displayed in Fig. 3A. Our classical simulation does not account for quantum interference effects, such as above-threshold ionization peaks. It is also important to note that the photoelectron emission angle is integrated over 4π, differing from simulations in stereo–above-threshold ionization–type experiments where CEP asymmetry, defined by left versus right emission, is highly sensitive to electron kinetic energy (*21*). In our angle-integrated case, the CEP dependence is not sensitive to the magnitude of electron kinetic energy but rather to its sign. In addition to being emitted with certain asymptotic kinetic energy, released electrons can be recaptured into excited bound states of the neutral molecule in the trailing part of the pulse. This strong-field excitation process is referred to as frustrated tunneling ionization (*22*, *23*). The two processes, photoemission and frustrated ionization, are compared in Fig. 3B as a function of the CEP. The ionized electron yield peaks at a CEP of 0, aligning with our experimental observation of CEP dependence in N_2^+ fluorescence. In contrast, the recaptured electron yield reaches a maximum for a sine-like pulse, consistent with previous theoretical studies (*24*, *25*). The total probability of recollision-induced excitation depends not only on the tunneling rate

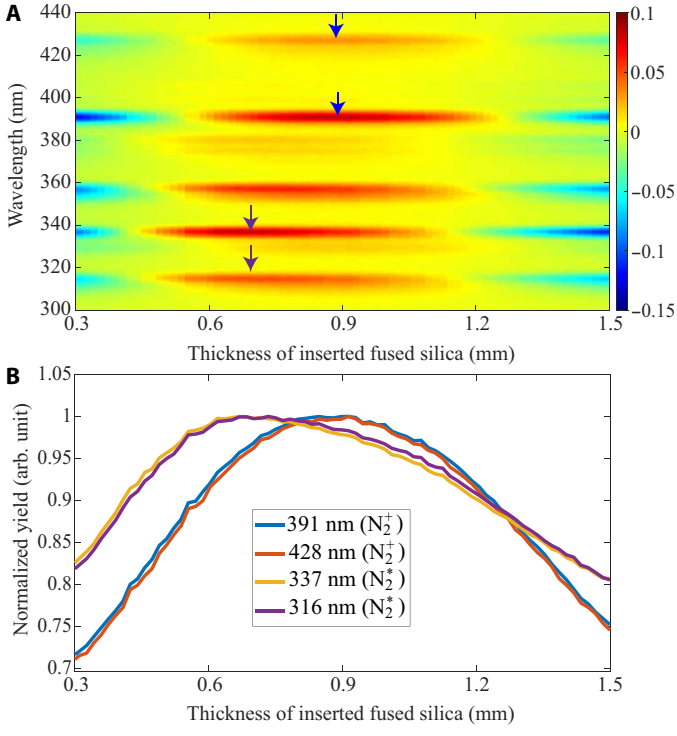

Fig. 2. Chirp dependence of air fluorescence. (**A**) Measured chirp-resolved differential distribution of the fluorescence spectrum, where the chirp is controlled by varying the thickness of inserted fused silica in the beam. (**B**) Several lineouts from (A) to highlight the different chirp dependence of the air fluorescence from N_2^+ and N_2^*. Note that the peak at 358 nm is slightly misaligned with those at 337 and 316 nm because of spectral congestion from the ionic signal (357 nm).

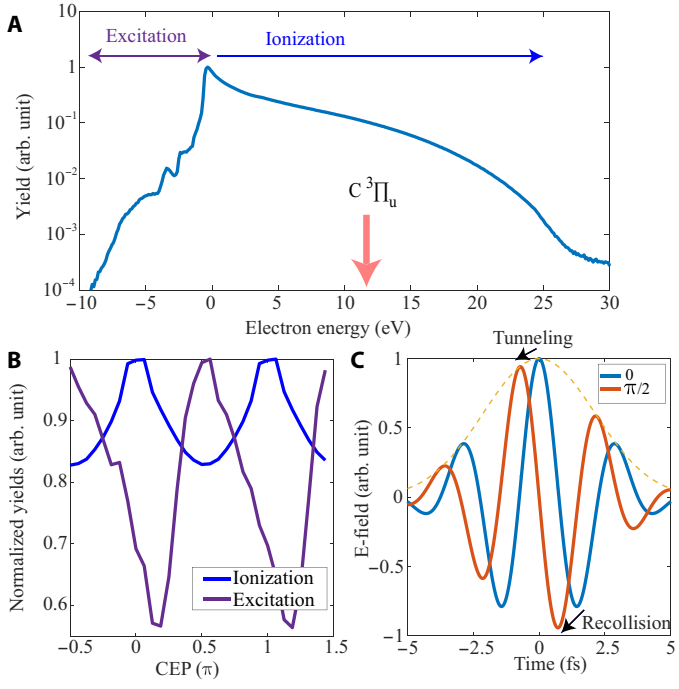

Fig. 3. Theoretical simulations for CEP dependence. (**A**) Simulated electron energy distribution in the logarithmic scale after interacting with an intense short pulse by the CTMC method. (**B**) Calculated CEP dependence of the yields of positive-energy electrons (ionization) and negative-energy electrons (excitation). (**C**) Comparison of the electric fields at the CEP of 0 and π/2. The dashed yellow line shows their envelope.

but also on the probability of recombinations. Figure 3C compares the electric field waveforms for CEP values of 0 and π/2. For the sine-like pulse, although the dominant electric field strength is slightly weaker, the electric field in the subsequent half-cycle—responsible for reversing electron velocity—increases substantially, enhancing the recombination probability. These results suggest that fluorescence from N_2^* primarily originates from the excited neutral pathway.

The chirp dependence of excitation and ionization from CTMC simulation, as shown in Fig. 4A, further supports this hypothesis. Using the refractive index of fused silica (*26*), we generated a chirp-free Gaussian-like pulse, passed it through fused silica, and seeded our CTMC simulation (*16*, *27*, *28*) with the resulting chirped pulses. Figure 4A displays the calculated ionization and excitation yields as a function of fused silica insertion. The simulation aligns with our experimental findings: Ionization is largely symmetric with respect to the pulse chirp sign, while excitation reaches a maximum under negative chirp conditions. When the pulse is chirped, it stretches in the time domain, reducing its peak intensity and thereby lowering the ionization yield. However, chirping also modifies the instantaneous frequency of the light pulse. Figure 4B compares the electric-field waveforms of chirp-free and negatively chirped pulses. After the peak, the electric field of the negatively chirped pulse stretches longer at the falling edge of the pulse, effectively shifting to a lower frequency. This extended wavelength range increases the quiver radius of ponderomotive motion, enhancing the recombination probability with parent ions. These results highlight that strong-field excitation depends not only on peak intensity but also on the subcycle structure of the electric field. Last, we emphasize that our interpretation focuses on the ability of the excited neutral pathway to explain the waveform-dependent observables—such as CEP dependence (with an observed contrast of ~1%) and chirp dependence (showing ~10% variation)—rather than asserting exclusivity over other mechanisms. While a correlation is observed between the coherent control of the waveform and the delayed formation of the $C^3\Pi_u$ state (after tens to a few hundred picoseconds), other mechanisms are likely involved during this timescale. Future studies involving additional observables or diagnostics may further clarify the relative contributions of different channels.

In conclusion, we have demonstrated that few-cycle waveform control via CEP and chirp enables the observation of distinct fluorescence behaviors from neutral N_2 molecules and N_2^+ ions. Our CTMC model corroborates these findings, supporting the excited neutral pathway as a consistent explanation for the CEP-dependent $C^3\Pi_u$ formation and showing how negatively chirped pulses enhance excitation via the trailing field, promoting frustrated tunneling ionization. These insights advance our understanding of strong-field excitation dynamics in air fluorescence and underscore the potential of ultrafast electric-field waveform control for probing complex molecular processes.

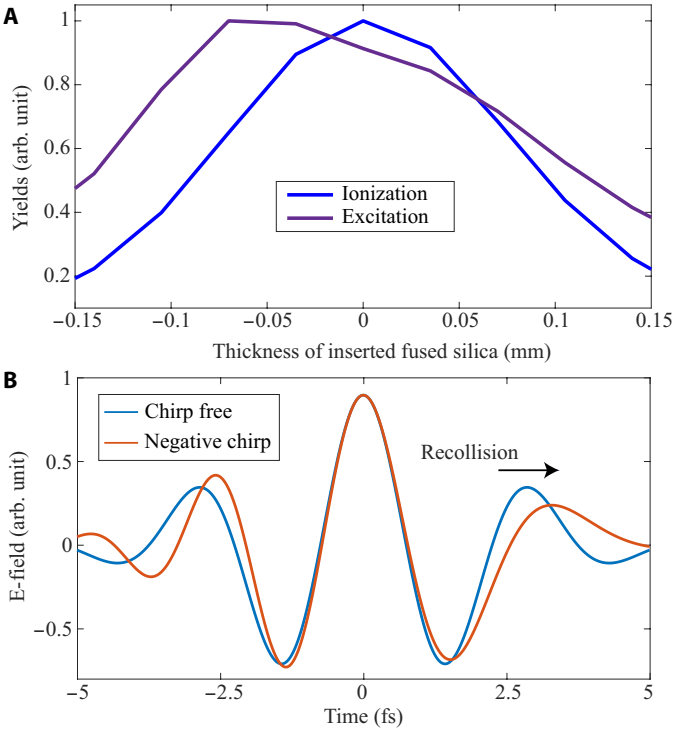

Fig. 4. Theoretical simulation of chirp dependence. (**A**) Calculated electron yields as a function of inserted fused silica in the beam. (**B**) Comparison of the electric fields of chirp-free and negatively chirped pulses. Note that the two pulses are shifted to overlap at time zero.

Supplementary Materials

This PDF file includes:

Figs. S1 and S2

Supplementary Text

REFERENCES AND NOTES

1. M. Ferray, A. L'Huillier, X. Li, L. Lompre, G. Mainfray, C. Manus, Multiple-harmonic conversion of 1064 nm radiation in rare gases. *J. Phys. B At. Mol. Opt. Phys.* **21**, L31–L35 (1988).
2. D. Cook, R. Hochstrasser, Intense terahertz pulses by four-wave rectification in air. *Opt. Lett.* **25**, 1210–1212 (2000).
3. M. Kress, T. Löffler, S. Eden, M. Thomson, H. G. Roskos, Terahertz-pulse generation by photoionization of air with laser pulses composed of both fundamental and second-harmonic waves. *Opt. Lett.* **29**, 1120–1122 (2004).
4. X. Xie, J. Dai, X.-C. Zhang, Coherent control of THz wave generation in ambient air. *Phys. Rev. Lett.* **96**, 075005 (2006).
5. J. S. Pearlman, G. H. Dahlbacka, Emission of rf radiation from laser-produced plasmas. *J. Appl. Phys.* **49**, 457–459 (1978).
6. Y. Brelet, A. Houard, G. Point, B. Prade, L. Arantchouk, J. Carbonnel, Y.-B. André, M. Pellet, A. Mysyrowicz, Radiofrequency plasma antenna generated by femtosecond laser filaments in air. *Appl. Phys. Lett.* **101**, (2012).
7. Q. Luo, H. Xu, S. Hosseini, J.-F. Daigle, F. Théberge, M. Sharifi, S. Chin, Remote sensing of pollutants using femtosecond laser pulse fluorescence spectroscopy. *Appl. Phys. B* **82**, 105–109 (2006).
8. A. Portnov, S. Rosenwaks, I. Bar, Emission following laser-induced breakdown spectroscopy of organic compounds in ambient air. *Appl. Optics* **42**, 2835–2842 (2003).
9. H. Xu, A. Azarm, J. Bernhardt, Y. Kamali, S. Chin, The mechanism of nitrogen fluorescence inside a femtosecond laser filament in air. *Chem. Phys.* **360**, 171–175 (2009).
10. H. Xu, A. Azarm, S. L. Chin, Controlling fluorescence from N_2 inside femtosecond laser filaments in air by two-color laser pulses. *Appl. Phys. Lett.* **98**, (2011).
11. R. Danylo, X. Zhang, Z. Fan, D. Zhou, Q. Lu, B. Zhou, Q. Liang, S. Zhuang, A. Houard, A. Mysyrowicz, E. Oliva, Y. Liu, Formation dynamics of excited neutral nitrogen molecules inside femtosecond laser filaments. *Phys. Rev. Lett.* **123**, 243203 (2019).
12. S. Mitryukovskiy, Y. Liu, P. Ding, A. Houard, A. Couairon, A. Mysyrowicz, Plasma luminescence from femtosecond filaments in air: evidence for impact excitation with circularly polarized light pulses. *Phys. Rev. Lett.* **114**, 063003 (2015).
13. W. Zheng, Z. Miao, C. Dai, Y. Wang, Y. Liu, Q. Gong, C. Wu, Formation mechanism of excited neutral nitrogen molecules pumped by intense femtosecond laser pulses. *J. Phys. Chem. Lett.* **11**, 7702–7708 (2020).
14. H. Mei, H. Jiang, A. Houard, V. Tikhonchuk, E. Oliva, A. Mysyrowicz, Q. Gong, C. Wu, Y. Liu, Fluorescence and lasing of neutral nitrogen molecules inside femtosecond laser filaments in air: Mechanism and applications. *Phys. Chem. Chem. Phys.* **26**, 23528–23543 (2024).

15. B. R. Arnold, S. D. Roberson, P. M. Pellegrino, Excited state dynamics of nitrogen reactive intermediates at the threshold of laser induced filamentation. *Chem. Phys.* **405**, 9–15 (2012).
16. B. HuP, J. Liu, S. Chen, Plateau in above-threshold-ionization spectra and chaotic behavior in rescattering processes. *Phys. Lett. A* **236**, 533–542 (1997).
17. M.-S. Tsai, A.-Y. Liang, C.-L. Tsai, P.-W. Lai, M.-W. Lin, M.-C. Chen, Nonlinear compression toward high-energy single-cycle pulses by cascaded focus and compression. *Sci. Adv.* **8**, eabo1945 (2022).
18. M. Han, M.-C. Chen, M.-S. Tsai, H. Liang, Hearing carrier-envelope offset frequency and phase in air with a microphone. *Optica* **12**, 459–464 (2025).
19. A. Baltuška, T. Udem, M. Uiberacker, M. Hentschel, E. Goulielmakis, C. Gohle, R. Holzwarth, V. S. Yakovlev, A. Scrinzi, T. W. Hänsch, F. Krausz, Attosecond control of electronic processes by intense light fields. *Nature* **421**, 611–615 (2003).
20. Y. Itikawa, Cross sections for electron collisions with nitrogen molecules. *J. Phys. Chem. Ref. Data Monogr.* **35**, 31–53 (2006).
21. G. G. Paulus, F. Lindner, H. Walther, A. Baltuška, E. Goulielmakis, M. Lezius, F. Krausz, Measurement of the phase of few-cycle laser pulses. *Phys. Rev. Lett.* **91**, 253004 (2003).
22. T. Nubbemeyer, K. Gorling, A. Saenz, U. Eichmann, W. Sandner, Strong-field tunneling without ionization. *Phys. Rev. Lett.* **101**, 233001 (2008).
23. U. Eichmann, S. Patchkovskii, "Frustrated tunneling ionization: Building a bridge between the internal and macroscopic states of an atom" in *Advances in Atomic, Molecular, and Optical Physics* (Elsevier, 2023), vol. 72, pp. 1–88.
24. W.-H. Xiong, X.-R. Xiao, L.-Y. Peng, Q. Gong, Correspondence of below-threshold high-order-harmonic generation and frustrated tunneling ionization. *Phys. Rev. A* **94**, 013417 (2016).
25. H. Yun, J. H. Mun, S. I. Hwang, S. B. Park, I. A. Ivanov, C. H. Nam, K. T. Kim, Coherent extreme-ultraviolet emission generated through frustrated tunnelling ionization. *Nat. Photon* **12**, 620–624 (2018).
26. I. H. Malitson, Interspecimen comparison of the refractive index of fused silica. *J. Opt. Soc. Am.* **55**, 1205–1209 (1965).
27. X. M. Tong, Z. X. Zhao, C. D. Lin, Theory of molecular tunneling ionization. *Phys. Rev. A* **66**, 033402 (2002).
28. A. C. Hindmarsh, "Odepack, a systemized collection of ode solvers" in *Scientific Computing* (North-Holland Publishing Company, 1983).

Acknowledgments: We thank C. Aikens, S. Chainey, and J. Millette for their technical support. **Funding:** The Kansas State group was supported by the Chemical Sciences, Geosciences and Biosciences Division, Office of Basic Energy Sciences, Office of Science, US Department of Energy, grant no. DE-FG02-86ER13491. The NTHU group was supported by the National Science and Technology Council, Taiwan, under grant no. 113-2112-M-007-042-MY3. **Author contributions:** M.H. conceived the study. M.-S.T., M.H., C.-C.T., and M.-C.C. performed the experiments. H.L. performed the simulations. M.H., H.L., U.T., and M.-C.C. analyzed and interpreted the data. All authors wrote the paper. **Competing interests:** The authors declare that they have no competing interests. **Data and materials availability:** All data needed to evaluate the conclusions in the paper are present in the paper and/or the Supplementary Materials.

Submitted 26 November 2024
Accepted 30 April 2025
Published 4 June 2025
10.1126/sciadv.adu9200